Ab initio investigation of electronic and vibrational contributions to linear and nonlinear dielectric properties of ice

S. Casassa, J. Baima, A. Mahmoud, and B. Kirtman

Citation: The Journal of Chemical Physics **140**, 224702 (2014); doi: 10.1063/1.4880961
View online: http://dx.doi.org/10.1063/1.4880961
View Table of Contents: http://scitation.aip.org/content/aip/journal/jcp/140/22?ver=pdfcov
Published by the AIP Publishing

Ab initio investigation of electronic and vibrational contributions to linear and nonlinear dielectric properties of ice

S. Casassa,[1] J. Baima,[1] A. Mahmoud,[1] and B. Kirtman[2]
[1]*Dipartimento Chimica IFM and Centre of Excellence NIS (Nanostructured Interfaces and Surfaces), Università degli Studi di Torino, via P. Giuria 5, I-10125 Torino, Italy*
[2]*Department of Chemistry and Biochemistry, University of California, Santa Barbara, California 93106, USA*

(Received 9 April 2014; accepted 20 May 2014; published online 11 June 2014)

Electronic and vibrational contributions to the static and dynamic (hyper)polarizability tensors of ice XI and model structures of ordinary hexagonal ice have been theoretically investigated. Calculations were carried out by the finite field nuclear relaxation method for periodic systems (FF-NR) recently implemented in the CRYSTAL code, using the coupled-perturbed Kohn-Sham approach (CPKS) for evaluating the required electronic properties. The effect of structure on the static electronic polarizabilities (dielectric constants) and second-hyperpolarizabilities is minimal. On the other hand, the vibrational contributions to the polarizabilities were found to be significant. A reliable evaluation of these (ionic) contributions allows one to discriminate amongst ice phases characterized by different degrees of proton-order, primarily through differences caused by librational motions. Transverse static and dynamic vibrational (hyper)polarizabilities were found by extrapolating calculations for slabs of increasing size, in order to eliminate substantial surface contributions. © *2014 AIP Publishing LLC*. [http://dx.doi.org/10.1063/1.4880961]

I. INTRODUCTION

The dielectric and conductive properties of ice have been extensively studied both experimentally and theoretically.[1–8] One of the many interesting anomalous properties is the high dielectric constant of ice Ih.[9] At the coexistence temperature, and 1 atm pressure, ice Ih has a larger dielectric constant than liquid water, even though it has a lower density. This property seems strictly related to the residual proton disorder that is well known[10] to persist at very low temperature. On the contrary, defects seem to have no bearing on the static dielectric properties: their concentration affects the rate at which ice responds to an applied field but not the final value of the polarization.[11,12]

The progress of the disorder-order transition in ice can be monitored by dielectric measurements, which can provide an insight into the mechanism whereby such reorganization proceeds. In fact, the low temperature ordering transition of ice Ih to ice XI, induced by doping with KOH, was first studied by this means.[13] It remains an open question as to whether or not dielectric relaxation can be seen as the driving force for proton reordering.[14]

This transition also produces micro-crystals with a unit cell that has a permanent dipole moment. The dielectric properties of the latter structure have been the object of many studies in the past[15,16] and are of interest here as well.

From a theoretical point of view, the reliability of classical models for H_2O used to simulate ice properties and to study order/disorder transitions is often tested through their ability to predict dielectric constants in good agreement with experiment.[6,7] Thus, there is considerable interest in the dielectric properties of ice crystals, as calculated from first principles in their own right, as well as in regard to their relationship with proton disorder.

In this work, we investigate the linear and nonlinear static dielectric, as well as electro-optical, properties of ice using periodic models, together with Kohn-Sham density functional theory (KS-DFT) including exact exchange. Both electronic and vibrational contributions are determined. Bearing in mind the most recent and complete first principle studies to date,[5,17,18] and with the support of the experimental findings,[19,20] we address several open questions: (i) can the calculated (hyper)polarizability tensors give a clear indication of the degree of (residual) proton disorder; (ii) through what means and by how much does spontaneous polarized structure affect the dielectric properties; (iii) what is the relative importance of the vibrational contribution; and (iv) how are these properties affected by dimensionality?

A. Methods

Static electronic (hyper)polarizabilities were calculated by means of the Coupled Perturbed Kohn-Sham (CPKS) DFT method, as implemented in the *ab initio* CRYSTAL code[21–23] which utilizes a basis set consisting of contracted Gaussian-type atomic orbitals (AO) functions. This same code was used to obtain vibrational contributions to the (hyper)polarizability[24] through the finite field nuclear relaxation (FF-NR) method,[25] a procedure based on geometry optimization in the presence of a static field (see Sec. II). The FF-NR method yields both static and dynamic (in the high frequency limit) vibrational (hyper)polarizabilities, that are correct through first-order in electrical and mechanical anharmonicity. In the current implementation, this method is limited to properties in non-periodic and mixed directions,[26,27] although results for periodic directions can be determined by extrapolation as we have done here. Within DFT, the

TABLE I. Ice structures employed in this paper. In addition to the space group we list the number of symmetry operators (Sym Op) and water molecules in the unit cell (n_{H_2O}) as well as the number of AOs (n_{AO}) in the *tzp*(*pol*) basis set (see Sec. III). CPU time, expressed in *hours*, refers to a complete CPKS job on a 32 processor Intel Xeon (2.13GHz). Each CPKS job includes a field-free SCF calculations and nine coupled-perturbed SCF calculations, three to obtain the first- and second-order susceptibility tensors and six to obtain the third-order susceptibility tensor.

	Space Group	Sym Op	n_{H_2O}	n_{AO}	CPU
P	P_{na2_1}	4	8	480	21
BF	C_{6mc}	12	12	720	23
XI	C_{mc2_1}	4	4	240	5

semi-local PBE functional, as well as hybrid B3LYP and B3LYP augmented by an empirical van der Waals term (i.e., B3LYP-D*) were employed.[28,29]

B. Ice models

Two bulk phases of ice were investigated, namely, ordinary hexagonal ice Ih and orthorhombic proton-ordered ice XI. Ice Ih, in turn, was modeled by two different periodic (long-range ordered) structures with unit cells of differing size that provide a variety of configurations to describe the local proton disorder. These structures, listed in Table I, are: (i) P_{na2_1} or P-ice, which has been extensively studied by one of us;[30,31] and (ii) the C_{6mc} unit cell proposed by Bernal and Fowler[32] (BF) and used, among others, by Murray and Galli.[18] P-ice has a smaller unit cell with respect to BF ice but also fewer symmetry operators and an asymmetric unit of six atoms, instead of five. Because the local environment of each irreducible oxygen presents a different proton distribution, P-ice exhibits a maximal configurational entropy and local disorder with respect to the other two structures. FF-NR vibrational (hyper)polarizabilities were determined for structure (i) by extrapolating results obtained for finite slabs of increasing thickness.

II. THEORY

The total energy of a system immersed in a static electric field $\boldsymbol{F}$ can be expanded in a power series (assuming the field is not too large),

$$E(\boldsymbol{F}) = E(0) - \sum_i \mu_i F_i - \frac{1}{2}\sum_{ij}\alpha_{ij}F_iF_j - \frac{1}{6}\sum_{ijk}\beta_{ijk} F_iF_jF_k - \frac{1}{24}\sum_{ijkl}\gamma_{ijkl}F_iF_jF_kF_l, \quad (1)$$

where the indices i, j, k, l refer to tensor components along the three Cartesian axes. The quantity μ is the permanent electric dipole moment, α is the linear polarizability, and β and γ are the first and second hyperpolarizabilities, respectively. These properties contain both an electronic, e, and a vibrational contribution, which we approximate at the nuclear relaxation, nr, level (see later). Experimentally, the former may be obtained by extrapolating high frequency measured values to the static limit. The static electronic (hyper)polarizabilities (and dipole moment) are defined by the pure electronic energy in Eq. (1) calculated at the field-free equilibrium geometry. These properties can be determined either by numerical differentiation or analytically by perturbation theory. Here we utilize the analytical Coupled Perturbed Kohn-Sham (CPKS) method,[33] as appropriately modified for periodic systems[34] and implemented in the CRYSTAL code.[35,36] CPKS takes into account orbital relaxation induced by the field and is known to be an efficient and reliable procedure for computing static electronic (hyper)polarizabilities of solid state systems.[22]

The vibrational contribution to the static (hyper)polarizabilities can also be obtained by perturbation theory using vibronic rather than pure electronic wavefunctions.[24] However, it is often more convenient to follow the finite field-nuclear relaxation (FF-NR) approach developed by Kirtman *et al.*[37,38] A version of the FF-NR method, that is applicable when electrical and mechanical anharmonicity is not too large, has been recently implemented in the CRYSTAL code.[27,39] This method was checked, in part, by comparing the FF-NR static vibrational linear polarizability with the (double harmonic) perturbation theory expression,

$$\alpha^{nr} \equiv \alpha^{v} = \sum_n \frac{\bar{Z}_n^2}{\nu_n^2}, \quad (2)$$

evaluated using a Berry phase like scheme for the mass weighted effective mode Born charge Z_n[40,41] and vibrational frequencies, ν_n, obtained by diagonalizing the dynamical matrix. The latter, in turn, was found by numerical differentiation of the analytical energy gradient.[35]

In addition, to provide static vibrational (hyper)polarizabilities, the FF-NR scheme in CRYSTAL allows one to obtain the high frequency limit (also known as the infinite optical frequency approximation) for the vibrational contribution to several dynamic nonlinear optical processes, namely, the dc-Pockels effect (dc-P), the dc-Kerr effect (dc-K), and field-induced second harmonic generation (dc-SHG). The procedure employed may be summarized as follows. We denote the relaxed equilibrium geometry in the presence of a static electric field by $\boldsymbol{R_F}$ and the field-free equilibrium geometry by $\boldsymbol{R_0}$. Then, we may define

$$(\Delta\pi)_{\boldsymbol{R_F}} = \pi(\boldsymbol{R_F}, \boldsymbol{F}) - \pi(\boldsymbol{R}_0, 0), \quad (3)$$

where $\pi = \mu, \alpha, \beta$ are calculated as pure electronic properties. For small values of the applied field each component of $\Delta\pi$ can be fit to a Taylor series expansion,

$$(\Delta\mu_i)_{\boldsymbol{R_F}} = a_1F_j + \frac{1}{2}b_1F_jF_k + \frac{1}{6}g_1F_jF_kF_l, \quad (4)$$

$$(\Delta\alpha_{ij})_{\boldsymbol{R_F}} = b_2F_k + \frac{1}{2}g_2F_kF_l + .., \quad (5)$$

$$(\Delta\beta_{ijk})_{\boldsymbol{R_F}} = g_3F_l + .., \quad (6)$$

where the directional indices on the expansion coefficients have been suppressed for convenience (cf. Eqs. (7)–(12) and the Einstein summation convention is assumed for the fields

on the right hand side (e.g., $a_1 F_j \equiv \sum_j \alpha_{ij} F_j$). The important point is that these coefficients can be identified with the *nr* approximation for the vibrational properties (at $\boldsymbol{R_0}$) mentioned above. This approximation is correct through the first-order of perturbation theory in mechanical and electrical anharmonicity. Thus, it turns out that

$$a_1 = \alpha^e_{ij}(0;0) + \alpha^{nr}_{ij}(0;0), \tag{7}$$

$$b_1 = \beta^e_{ijk}(0;0,0) + \beta^{nr}_{ijk}(0;0,0), \tag{8}$$

$$g_1 = \gamma^e_{ijkl}(0;0,0,0) + \gamma^{nr}_{ijkl}(0;0,0,0), \tag{9}$$

and

$$b_2 = \beta^e_{ijk}(0;0,0) + \beta^{nr}_{ijk}(-\omega;\omega,0), \tag{10}$$

$$g_2 = \gamma^e_{ijkl}(0;0,0,0) + \gamma^{nr}_{ijkl}(-\omega;\omega,0,0), \tag{11}$$

$$g_3 = \gamma^e_{ijkl}(0;0,0,0) + \gamma^{nr}_{ijkl}(-2\omega;\omega,\omega,0). \tag{12}$$

In Eqs. (7)–(12), we have used the standard notation for the frequencies-dependent properties, e.g., $\gamma^{nr}_{ijkl}(-\omega;\omega,0,0) = \gamma^{nr}_{ijkl}(-\omega_\sigma;\omega_j,\omega_k,\omega_l)$ with ω_j, ω_k, ω_l being the frequencies of external fields F_j, F_k, F_l, respectively, and $\omega_\sigma = \omega_j + \omega_k + \omega_l$. Moreover, these expressions are valid only in the high-frequency limit, formally when $\omega \to \infty$, which is effectively the case (or nearly the case) for most experimental measurements (vibrational frequencies are negligible compared to optical frequencies). Finally, if $\boldsymbol{R_F}$ in Eq. (3) is replaced by $\boldsymbol{R_0}$, the coefficients in Eqs. (7)–(12) reduce to the pure static electronic term.

It is worth noting that the larger the number of static external fields the greater, in general, will be the *nr* property value as compared to the corresponding static electronic contribution. For example, it is often true that the second term on the right-hand side (rhs) of Eq. (9), which has 3 static external fields, is much larger than the first term. Even for properties involving only one static external field (static α, dc-P, dc-SHG), it has been found that the *nr* contribution can be quite important.

We will be interested in extrapolating the calculated (hyper)polarizabilities of 2D periodic slabs, with an increasing number of layers, to the bulk ice limit. In order to convert the microscopic property values to macroscopic susceptibilities, χ, for components along the perpendicular (non-periodic) z-direction, one needs to take into account the difference between the microscopic (displacement) field and the macroscopic field. If the fields were the same, then the desired relations would be simply:

$$\epsilon_{ij} = 1 + \chi_{ij} = 1 + \frac{4\pi}{V}\alpha_{ij}, \tag{13}$$

$$\epsilon_{ijk} = \chi_{ijk} = \frac{2\pi}{V}\beta_{ijk}, \tag{14}$$

$$\epsilon_{ijkl} = \chi_{ijkl} = \frac{2\pi}{3V}\gamma_{ijkl}, \tag{15}$$

with V equal to the unit cell volume. For slabs, however, the macroscopic field (outside the material) differs from the displacement field. As a consequence, the expression for the component of the dielectric tensor in the non-periodic direction is

$$\epsilon_{zz} = \frac{1}{1 - (4\pi\alpha_{zz}/V)} \tag{16}$$

and when the z index appears n times in Eqs. (14) or (15) one must multiply on the rhs by $(\epsilon_{zz})^n$.

III. COMPUTATIONAL DETAILS

The choice of functional, basis set, and main computational parameters were carefully checked in order to ensure accuracy within the CPKS and FF-NR methodologies that were employed. In doing so, we have relied to a large extent on previous work.[27,29,39]

As far as the functional is concerned, it is well-known that the local density and generalized gradient approximations (LDA and GGA) often strongly overshoot the (hyper)polarizability, in large part because of an inadequate description of electron exchange.[42,43] Thus, we have chosen to use the B3LYP functional, which includes 20% exact exchange and yields significantly improved results - although still with some tendency to overshoot. In order to account for dispersion, the B3LYP-D* functional was also employed. The latter augments B3LYP with damped empirical dispersion terms of the form $-f(\boldsymbol{R})C_6/\boldsymbol{R}^6$, as originally proposed by Grimme[28] and recently implemented in the CRYSTAL code.[29] Finally, in order to compare our results with those of Galli *et al.*,[18] PBE calculations were also performed.

For molecules, the accurate calculation of hyperpolarizabilities requires, in general, the use of a basis set with diffuse and polarization functions. In the case of periodic systems, diffuse functions can lead to numerical problems due to linear dependence and, as it turns out, they are not mandatory. In our case, we started from a standard triple-zeta plus polarization basis (*tzp*), then split the polarization function and included another polarization function of higher angular momentum. Thus, for oxygen the *d* shell, with exponent $\alpha_d = 1.2$, was split into two shells with $\alpha_{d_1} = 2.314$ and $\alpha_{d_2} = 0.645$. Beyond that an *f* shell with $\alpha_f = 1.428$ was added. For hydrogen the *p* shell in the original *tzp* basis set, with $\alpha_p = 0.8$, was split into two shells with exponents $\alpha_{p_1} = 1.407$ and $\alpha_{p_2} = 0.388$, and a *d* shell was added with $\alpha_d = 1.057$. Our resulting basis set is referred to in the following as *tzp*(*pol*).

In order to check the convergence with respect to basis set size two other basis sets were constructed. For the first one, named *tzp*($pol - d3$), a further polarization function was added on each atom, so that the exponent of the most diffuse polarization function was $\alpha_{p_3} = 0.207$ for hydrogen and $\alpha_{d_3} = 0.352$ for oxygen. The second was obtained by augmenting the *tzp*(*pol*) basis set with the (most) diffuse polarization functions $\alpha_{p_3} = 0.129$ and $\alpha_{d_2} = 0.33$ for hydrogen, $\alpha_{d_3} = 0.214$ and $\alpha_{f_2} = 0.5$ for oxygen and is referred as *tzp*($aug - pol$).

In polymer and nanotube calculations it has been shown[39,44] that there are just a few computational

parameters that exert an important influence on the calculated (hyper)polarizability tensor. One of them is the number of **k** points in reciprocal space, n_k, for which the field-free SCF and CPKS equations are solved. This number is determined by the shrinking factor, S, which we have set equal to 8. For the relationship between S and n_k, as well as for the other computational parameters given below, please refer to the CRYSTAL Manual.[45] Another important parameter is the number of terms in the Hartree-Fock exchange series, which is controlled by tolerances on the integrals, T_4^i and T_5^i, for which we have adopted the values of 10 and 18, respectively. The convergence thresholds for the field-free SCF energy and the solution of the CPKS perturbation equations were set to $T_{SCF}^E = 12$ and $T_{CPKS}^E = 4$.[44] Finally, in geometry optimizations within the FF-NR procedure the convergence threshold, based on the root mean square gradient of the total energy, was set to 10^{-5} a.u. (30 times lower than the default value).

IV. RESULTS

A. Bulk

All structures were fully optimized and binding energies were evaluated taking into account the basis set superposition error.[46,47] The relative stability in the low pressure regime at $T \approx 0$, given by $\Delta G(0, 0)$, was obtained by adding the zero point energy correction in the harmonic oscillator approximation. Although the energy differences are small at the B3LYP/*tzp*(*pol*) level, the most stable of the three ice structural models considered was calculated to be ice XI with the least stable being BF ice. The same procedure was followed using several different functionals: PBE0,[48] PBE, as well as dispersion corrected[29] B3LYP-D* and PBE0-D*. In each case, ice XI was predicted to be the most stable phase, despite some significant differences in the geometric parameters. Our B3LYP/*tzp*(*pol*) results for binding energy, $\Delta G(0, 0)$, unit cell volume (V), bulk modulus (B_0), and pressure derivative of B_0 (B_0') are reported in Table II along with experimental values for ice Ih and those computed by Murray and Galli[18] for ice XI using a non-local van der Waals functional (vdW-DF2). Our calculations and those of Murray and Galli give comparable overall agreement with experiment. In the latter comparison we assume that, *for the properties in Table II*, the differences between ice XI and ice Ih are essentially negligible, as our calculations show.

TABLE II. Binding energy per water molecule, equilibrium volume per mole, bulk modulus (B_0) and its dimensionless pressure derivative (B_0') calculated at the B3LYP/*tzp*(*pol*) level for ice XI and the two ice Ih models, P, and BF.

	XI	P	BF	XI[a]	Expt.[b]
$E_{binding}$ [eV]	− 0.563	− 0.561	− 0.560	− 0.649	− 0.610
$\Delta G(0, 0)$	− 0.496	− 0.487	− 0.486	− 0.520	− 0.491
V [cm^3/mol]	19.43	19.46	19.47	20.01	19.30
B_0 [GPa]	12.73	12.59	12.68	12.59	12.1
B_0'	5.5	5.5	5.6	5.2	5.5

[a]Calculations by Murray and Galli[18] using a non-local van der Waals functional (vdW-DF2) with a plane wave basis set.
[b]Data for ice Ih from Ref. 19.

TABLE III. Average static electronic ϵ^e, vibrational nuclear relaxation $\langle\epsilon^{nr}\rangle$, and total $\langle\epsilon^0\rangle$ dielectric constants, in a.u., for different ice polymorphs. All calculations were carried out with the *tzp*(*pol*) basis set, unless otherwise indicated. Our results for ice XI are compared with those obtained by Murray and Galli.[18]

		$\langle\epsilon^e\rangle$	$\langle\epsilon^0\rangle$	$\langle\epsilon^{nr}\rangle$
XI	B3LYP	1.65	2.58	0.93
	B3LYP-D*	1.68	2.62	0.94
	vdW-DF2[18]	1.78	2.55	0.77
	PBE	1.78	2.92	1.15
	PBE[18]	1.83	2.87	1.04
	PBE, *tzp(pol-d3)*	1.82	2.97	1.15
	PBE, *tzp(aug-pol)*	1.84	3.01	1.17
	PBE0	1.68	2.66	0.98
BF	B3LYP	1.65	2.74	1.09
	B3LYP-D*	1.68	2.79	1.11
	PBE	1.78	3.14	1.37
	PBE0	1.67	2.85	1.17
P	B3LYP	1.65	2.80	1.15
	B3LYP-D*	1.68	2.85	1.17
	PBE	1.78	3.24	1.46
	PBE0	1.67	2.90	1.23
I_h	Expt.[1,50]	1.72	3.09	1.37

Static electronic (hyper)polarizability tensors were calculated at the optimized geometry for the BF, P, and ice XI models at the B3LYP/*tzp*(*pol*) level. The (orientational) average static dielectric constants are reported in Table III whereas elements of the static first- and second-order dielectric tensors (see Eqs. (13)–(15)) are reported in Table IV. In Table III, we also present the average *nr* vibrational contribution, as determined by the Berry phase approach (see Eq. (2)) as well as the average total (electronic+vibrational) static dielectric constant. In addition, Table III contains PBE, PBE0, and B3LYP-D* results obtained with the *tzp*(*pol*) basis and, for ice XI, PBE was used with larger basis sets as well. The geometries were optimized separately for each level of calculation.

As far as the pure electronic dielectric constant in Table III is concerned there is no distinction between the three different ice models. Furthermore, there is no anisotropy: the diagonal elements of $\langle\epsilon^e\rangle$ are all the same. There is, of course,

TABLE IV. First- and second-order dielectric constants evaluated at the B3LYP/*tzp*(*pol*) level. See Eqs. (14) and (15) for the definition of these quantities.

	XI	P	BF
ϵ^e_{xxz}	0.372	− 0.003	0.132
ϵ^e_{yyz}	− 0.103	0.0	0.132
ϵ^e_{zzz}	0.804	− 0.002	0.817
ϵ^e_{xxxx}	30.0	29.69	29.58
ϵ^e_{xxyy}	10.45	9.51	9.86
ϵ^e_{xxzz}	8.29	7.39	7.73
ϵ^e_{yyyy}	29.3	29.27	29.58
ϵ^e_{yyzz}	7.39	7.91	7.73
ϵ^e_{zzzz}	35.0	34.17	34.49

a dependence upon the functional and basis set, but not on the ice structure, i.e., not on the long-range proton ordering. This is, perhaps, not unexpected since the electronic structure is very similar in the three cases despite the spontaneous polarization of ice XI.

The effect of dispersion is small, which may be inferred by comparing B3LYP with B3LYP-D* for ice XI. From our ice XI PBE calculations, using three different basis sets, we also conclude that the effect of increasing the size of the basis is small (less than 4%) confirming the satisfactory use of *tzp*(*pol*). The larger basis set calculations could not be done for B3LYP or B3LYP-D* because of convergence problems. However, we note that a comparable 3%-4% increase would bring our calculated value of $\langle\epsilon^e\rangle$ in very close agreement with experiment. A small difference between our PBE result and the one obtained by Murray and Galli[18] can probably be explained by the use of different basis sets. The PBE overshoot (see discussion at beginning of Sec. III), although small for ice, can be assigned to an inadequate description of electron exchange, which is consistent with the smaller value obtained at the PBE0 level, ($\langle\epsilon^e\rangle = 1.67$ vs 1.78).

There is an important vibrational contribution to the average static dielectric constant. In contrast with the electronic term, it depends significantly on the long-range proton ordering. Upon passing from ice XI to P-ice, the most disordered structure, this contribution varies from 0.93 a.u. (corresponding to 36% of the entire value) to 1.15 a.u. (41%) in the B3LYP calculations. The experimental value of 1.37 a.u. for ice Ih is considerably larger than that calculated for the P and BF models. On the other hand, the PBE values for these models are much closer to experiment. The PBE, B3LYP, and PBE0 functionals all show a very roughly comparable increase upon going from ice XI to BF-ice and P-ice.

In a recent article, Shigenari and Abe[49] pointed out that, while stretching (and other) vibrational frequencies above 1200 cm^{-1} vary insignificantly from ice Ih to ice XI, there are notable differences in the librational modes between 600 and 1100 cm^{-1}. This observation is consistent with the B3LYP/*tzp*(*pol*) IR spectra that we have calculated for P, BF, and ice XI structures. After dividing our calculated intensity by the square of the vibrational frequency[24] and summing over the librational modes, we find that the *differences* in the predicted *nr* dielectric constants are close (within 6%) to those reported in Table III. Thus, we predict a significant difference between ice XI (not yet measured) and ice Ih, that can be assigned to the librational modes.

The first- and second-order B3LYP/*tzp*(*pol*) static dielectric constants (equal to the second- and third-order susceptibility tensors) are given in Table IV. For the bulk, we show only the pure electronic values; the FF-NR vibrational contributions, obtained from slab calculations, will be reported in Subsection IV B. In third-order the diagonal electronic susceptibility, values are 3-5 times larger than the off-diagonal values. For all components, however, there are relatively small differences between the three different structural models. Our results for B3LYP-D* and PBE show the same general behavior. On the contrary, the components of the second-order susceptibility tensor, which depend on the non-centrosymmetric electronic response, vary strongly from one crystalline structure to another. This tensor vanishes for orthorhombic P-ice, since it is centrosymmetric, while BF-ice is perfectly isotropic in the *xy* plane.

B. Slab

The FF-NR method was employed with ice slabs of increasing thickness to evaluate the vibrational contribution to static and dynamic (hyper)polarizabilities in the nuclear relaxation approximation. Bulk properties were then obtained by extrapolating to the infinite slab limit. We selected the P structure to model the ice slab because it has local disorder, yet forms a simple (001) surface with no dipole component perpendicular to it, and essentially no dipole component parallel to it either.[30,51] As explained in Ref. 52, this choice is a natural one also in the light of accurate LEED studies.[53] On the contrary, surfaces cut out from ice XI exhibit a catastrophic instability with increasing size as a consequences of the net dipole perpendicular to the surface.[52]

Slabs of increasing thickness were cut out from bulk, along the (001) direction, i.e., perpendicular to the *z*-axis. An *n*-slab is defined to consist of *n* molecular layers with 4*n* water molecules in the unit cell as shown in Fig. 1 for $n = 2$. Regardless of the value of *n* all such slabs have the same surface geometry.

The energy and dielectric properties were evaluated for slabs with even *n*, for $n = 2$ to $n = 8$. Surface contributions to macroscopic properties vanish slowly, i.e., as $1/n$, but can be removed by carefully fitting the data. In addition, one must convert from the microscopic field used in slab calculations to the bulk macroscopic field as discussed in Sec. II.

As an initial test we evaluated the field-free total energy, as well as the static electronic dielectric constant and third-order susceptibility (= second-order dielectric) tensors. The bulk limit was obtained by fitting the data with a second order polynomial in $1/n$. Our results are reported in Table V where the bulk values from Tables III and IV are also shown for sake of comparison. It can readily be seen that the fitted results are in good agreement with those calculated for the bulk structure, with a maximum difference of 2% for ϵ^e_{zzzz}.

The FF-NR method was subsequently applied to obtain dynamic (infinite optical frequency approximation), as well as static, vibrational linear and nonlinear optical properties. The values of the field were chosen to be small enough to minimize effects from higher order energy derivatives and to

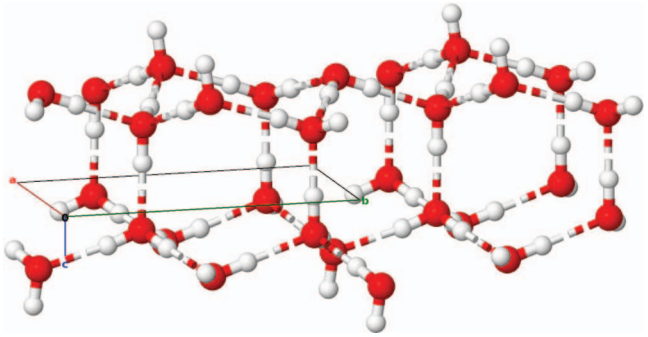

FIG. 1. Example of P-ice surface for $n_{slabs} = 2$. Periodicity along the *a* and *b* directions is maintained.

TABLE V. Total energy (in eV) as well as components of the electronic dielectric constant and third-order susceptibility tensors per water molecule in a slab of n layers, with $n = 2, 4, 6, 8$. Reported values were obtained at the B3LYP/*tzp*(*pol*) and fitted to a polynomial in $1/n$ to obtain the bulk limit. In the last column the corresponding quantities for P-ice bulk are given.

n_{slabs}	2	4	6	8	Limit	Bulk
$\Delta E - E_{bulk}$	2.462	0.906	0.128	0.096	−0.012	...
ϵ^e_{xx}	1.66	1.66	1.66	1.66	1.66	1.66
ϵ^e_{yy}	1.63	1.64	1.64	1.65	1.65	1.65
ϵ^e_{zz}	1.60	1.63	1.64	1.64	1.65	1.65
ϵ^e_{xxxx}	31.24	30.49	30.46	30.35	30.15	29.68
ϵ^e_{xxyy}	9.33	9.46	9.48	9.50	9.51	9.51
ϵ^e_{xxzz}	6.87	7.10	7.18	7.23	7.34	7.38
ϵ^e_{yyyy}	27.58	28.45	28.74	28.87	29.28	29.22
ϵ^e_{yyzz}	6.33	7.16	7.38	7.51	7.92	7.91
ϵ^e_{zzzz}	23.60	28.64	30.20	31.08	33.45	34.17

avoid convergence problems in the SCF procedure. To obtain reliable results the parameters controlling numerical accuracy had to be increased to very high values, especially for the SCF and geometry optimization procedures (see Sec. III). Fits of the electric field dependence for two representative electronic properties (dipole moment; polarizability along z) obtained using the $n = 2$ slab are shown in Fig. 2. The mean uncertainty

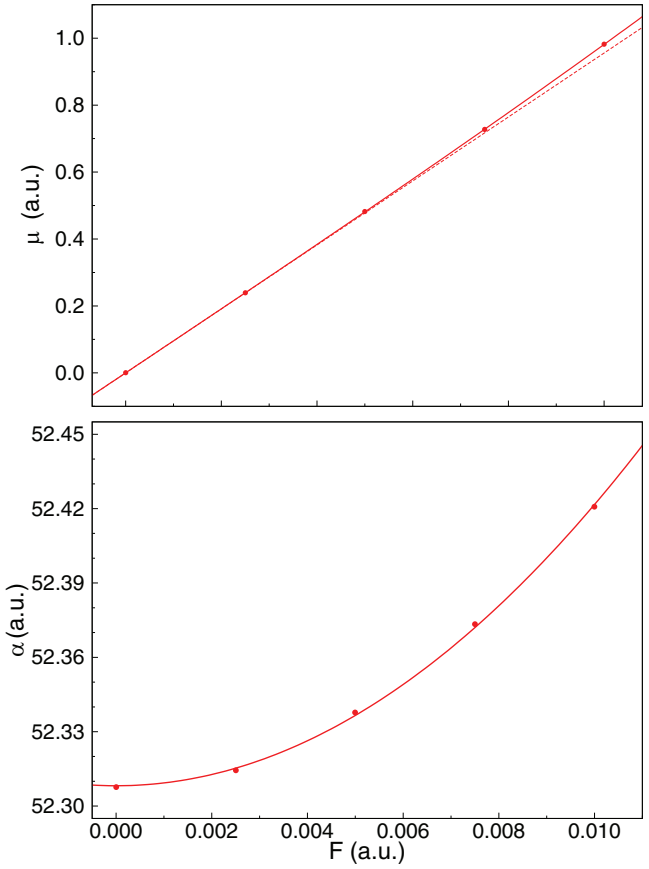

FIG. 2. Top panel: Electronic dipole moment perpendicular to the slab as a function of the finite field **F** at the optimized field-dependent geometry. The fitting function is a third-order odd polynomial and the dashed line represents the linear behavior $\boldsymbol{\mu} = \alpha \mathbf{F}$. Bottom panel: Electronic polarizability perpendicular to slab; the fitting function is a quadratic polynomial.

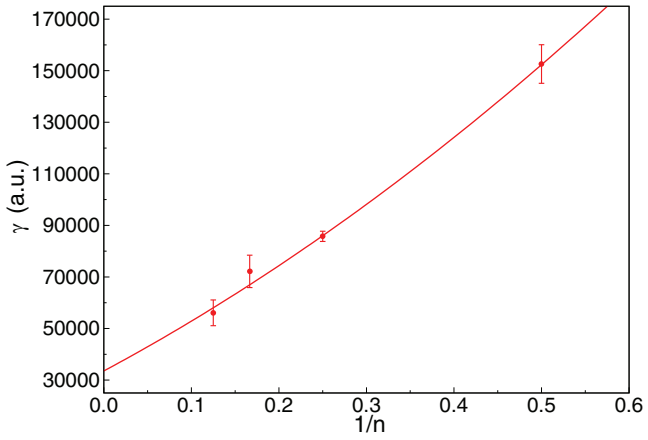

FIG. 3. Static vibrational (nuclear relaxation) second hyperpolarizability as a function of the inverse of the slab thickness $1/n$. Values were obtained by the FF-NR method at the B3LYP/*tpz*(*pol*) level. The fitting function is a quadratic polynomial in $1/n$, and the extrapolated bulk value corresponds to $1/n = 0$.

in the fitted property values is below 3%; for the static γ the uncertainties are shown as error bars in Fig. 3.

The nuclear relaxation dielectric properties, summarized in Table VI, show a much larger dependence on slab thickness than the corresponding pure electronic properties. This is due to the fact that breaking hydrogen bonds at the surface has a much larger effect on the vibrational parameters. The nuclear relaxation results obtained for the $n = 2$ slab often deviate from the trend of the thicker ones. In that connection, we note that for $n = 2$ all the water molecules belong either to the top or to the bottom surface, without any "bulk" in between. Even for thicker slabs, surface contributions to the static nonlinear dielectric properties are important. Their behavior is, however, well described by a polynomial fit in $1/n$, as seen in Fig. 3, which allows a reliable extrapolation to the bulk value. As an additional test of the reliability of the method, we can compare the value obtained for $\epsilon^0_{zz} = 2.87$ with the bulk result calculated using Eq. (2), $\epsilon^0_{zz} = 2.88$.

The static second-order vibrational dielectric constant in the z direction $\epsilon^0_{zzzz} = 2730$ is 80 times larger than the corresponding pure electronic property $\epsilon^e_{zzzz} = 34.2$ (see Table V). This ratio is not unexpected, given the strongly polar hydrogen-bonded nature of the ice crystal, but still quite remarkable. Both the field-induced vibrational

TABLE VI. B3LYP/*tpz*(*pol*) nuclear relaxation (hyper)polarizabilities obtained by the FF-NR method for different n-slabs of P-ice, with $n = 2$-8. Values are normalized with respect to the number of molecules in the periodic unit cell of $n = 2$ slab to show the convergence to bulk values.

n_{slabs}	2	4	6	8	Limit	ϵ
$\alpha_{zz}(0; 0)$	95.58	94.71	93.03	92.68	90.44	2.87
$\gamma_{zzzz}(0; 0, 0, 0)$	152600	85757	72165	56080	33545	2731
$\gamma_{xxzz}(-\omega; \omega, 0, 0)$	4983	2532	1872	1810	1361	13.4
$\gamma_{yyzz}(-\omega; \omega, 0, 0)$	1326	1078	1257	1664	1967	19.4
$\gamma_{zzzz}(-\omega; \omega, 0, 0)$	2269	2392	2272	2215	2089	56.2
$\gamma_{xxzz}(-2\omega; \omega, \omega, 0)$	563	704	763	789	872	4.70
$\gamma_{xyzz}(-2\omega; \omega, \omega, 0)$	66	66	34	25	0	0
$\gamma_{yyzz}(-2\omega; \omega, \omega, 0)$	1438	1532	1457	1443	1374	7.41
$\gamma_{zzzz}(-2\omega; \omega, \omega, 0)$	1287	1459	1574	1627	1779	27.5

second harmonic generation (ESHG^{nr}, $\gamma_{zzzz}(-2\omega; \omega, \omega, 0)$ in Table VI) and the vibrational electro-optical Kerr effect (EOKE^{nr}, $\gamma_{zzzz}(-\omega; \omega, 0, 0)$ in Table VI) have values of the same order of magnitude as the electronic response; EOKE^{nr} is very roughly twice as large, whereas ESHG^{nr} is very roughly the same. These results confirm that vibrations make a major contribution to the nonlinear dielectric properties of ice even for (field-induced) dynamic properties such as ESHG and EOKE.

V. CONCLUSIONS

The electronic and vibrational contributions to the linear polarizability and (second) hyperpolarizability tensors of ice Ih have been evaluated by means of the CPKS/FF-NR scheme at the B3LYP/*tzp*(*pol*) level. Two models were adopted, namely, the orthorombic P_{na2_1} and the Bernal-Fowler C_{6mc} structures. Our computed values have been compared with ice XI calculations done by ourselves and others, and with experimental results, where available.

It has been shown that the vibrational contribution to the static polarizability allows one to discriminate amongst the various hydrogen patterns, i.e., the degree of residual proton disorder in the ice phases. The differences are associated with librational motions.

Ice XI and BF-ice differ from P-ice in the lack of inversion symmetry, which give rise to a dipole moment, i.e., spontaneous polarization, as well as a non-vanishing first hyperpolarizability. Nonetheless, the electronic linear polarizability and second hyperpolarizability tensors are quite similar. There is a difference of about 20% in the vibrational contribution to the static linear polarizability (about 8% in the total value). Unfortunately, the effect of the polarized structure on the vibrational (hyper)polarizabilities could not be determined.

Bulk values for the vibrational contribution to dynamic (infinite optical frequency approximation) as well as static, processes were obtained for P-ice by extrapolation of FF-NR calculations on slabs of increasing thickness. In these calculations, the geometry of the slab is optimized in the presence of a finite field perpendicular to the surface simulated by cutting the bulk along the (001) plane. Then, the variation of electronic dipole moment and dielectric susceptibilities is evaluated as a function of field at the field-dependent relaxed geometry. It turns out that vibrational contributions dominate the amplitude of the static second-order dielectric properties, and are roughly as important as the electronic contributions for the ESHG and EOKE processes.

Finally, surface effects strongly influence the vibrational contribution to dielectric properties, especially the nonlinear ones, as opposed to electronic contributions which appear very similar in bulk and slab structures.

ACKNOWLEDGMENTS

Computing facilities from CINECA (project *IsC08_FPHC*) are gratefully acknowledged.

[1]G. Johari and S. Jones, Proc. R. Soc. A **349**, 467 (1976).
[2]G. Johari, J. Chem. Phys. **64**, 3998 (1976).
[3]I. Takei and N. Maeno, J. Phys. Chem. B **101**, 6234 (1997).
[4]V. F. Petrenko and R. W. Whitworth, *Physics of Ice* (Oxford University Press, Oxford, England, 1999), Chap. 4, p. 60.
[5]H. Reis, S. Raptis, and M. Papadopoulos, Chem. Phys. **263**, 301 (2001).
[6]W. Rick and A. Haymet, J. Chem. Phys. **118**, 9291 (2003).
[7]L. G. MacDowell and C. Vega, J. Phys. Chem. B **114**, 6089 (2010).
[8]A. Zaretskii, R. Howe, and R. Whitworth, Philos. Mag. B **63**, 757 (1991).
[9]N. Fletcher, *The Chemical Physics of Ice* (Cambridge University Press, Cambridge, England, 1970).
[10]L. Pauling, J. Am. Chem. Soc. **57**, 2680 (1935).
[11]D. Adams, Nature (London) **293**, 447 (1981).
[12]L. Onsanger and L. Runnels, J. Chem. Phys. **50**, 1089 (1969).
[13]S. Kawada, I. Take, and H. Abe, J. Phys. Soc. Jpn. **58**, 54 (1989).
[14]M. Tyagi and S. Murthy, J. Phys. Chem. A **106**, 5072 (2002).
[15]G. Johari and E. Whalley, J. Chem. Phys. **75**, 1333 (1981).
[16]S. Kawada and H. Dota, J. Phys. Soc. Jpn. **54**, 477 (1985).
[17]D. Lu, F. Gygi, and G. Galli, Phys. Rev. Lett. **100**, 147601 (2008).
[18]E. D. Murray and G. Galli, Phys. Rev. Lett. **108**, 105502 (2012).
[19]E. Whalley, J. Chem. Phys. **81**, 4087 (1984).
[20]Y. Yoshimura, S. Stewart, M. Somayazulu, H. K. Mao, and R. Hemley, J. Chem. Phys. **124**, 024502 (2006).
[21]M. Ferrero, M. Rerat, R. Orlando, and R. Dovesi, J. Comput. Chem. **29**, 1450 (2008).
[22]M. Ferrero, M. Rerat, R. Orlando, and R. Dovesi, J. Chem. Phys. **128**, 014110 (2008).
[23]M. Ferrero, M. Rerat, B. Kirtman, and R. Dovesi, J. Chem. Phys. **129**, 244110 (2008).
[24]D. M. Bishop and B. Kirtman, J. Chem. Phys. **95**, 2646 (1991).
[25]D. M. Bishop, M. Hasan, and B. Kirtman, J. Chem. Phys. **103**, 4157 (1995).
[26]V. Lacivita, M. Rerat, B. Kirtman, R. Orlando, M. Ferrabone, and R. Dovesi, J. Chem. Phys. **137**, 014103 (2012).
[27]M. Ferrabone, B. Kirtman, V. Lacivita, M. Rerat, R. Orlando, and R. Dovesi, Int. J. Quantum Chem. **112**, 2160 (2012).
[28]S. Grimme, J. Comput. Chem **27**, 1787 (2006).
[29]B. Civalleri, C. M. Zicovich-Wilson, L. Valenzano, and P. Ugliengo, CrystEngComm **10**, 405 (2008).
[30]C. Pisani, S. Casassa, and P. Ugliengo, Chem. Phys. Lett. **253**, 201 (1996).
[31]A. Erba, S. Casassa, R. Dovesi, L. Maschio, and C. Pisani, J. Chem. Phys. **130**, 074505 (2009).
[32]J. D. Bernal and R. Fowler, J. Chem. Phys. **1**, 515 (1933).
[33]G. J. B. Hurst and M. Dupuis, J. Chem. Phys. **89**, 385 (1988).
[34]B. Kirtman, F. L. Gu, and D. M. Bishop, J. Chem. Phys. **113**, 1294 (2000).
[35]M. Ferrero, M. Rerat, R. Orlando, R. Dovesi, and I. Bush, J. Phys.: Conf. Ser. **117**, 012016 (2008).
[36]R. Orlando, M. Ferrero, M. Rerat, B. Kirtman, and R. Dovesi, J. Chem. Phys. **131**, 184105 (2009).
[37]B. Kirtman, J. M. Luis, and D. M. Bishop, J. Chem. Phys. **108**, 10008 (1998).
[38]B. Kirtman and J. M. Luis, J. Chem. Phys. **128**, 114101 (2008).
[39]M. Ferrabone, B. Kirtman, M. Rerat, R. Orlando, and R. Dovesi, Phys. Rev. B **83**, 235421 (2011).
[40]R. Resta, Rev. Mod. Phys. **66**, 899 (1994).
[41]S. Dall'Olio, R. Dovesi, and R. Resta, Phys. Rev. B **56**, 10105 (1997).
[42]B. Champagne, E. A. Perpète, S. J. A. van Gisbergen, E. J. Baerends, J. G. Snijders, C. Soubra-Ghaoui, K. A. Robins, and B. Kirtman, J. Chem. Phys. **109**, 10489 (1998).
[43]B. Kirtman, V. Lacivita, R. Dovesi, and H. Reis, J. Chem. Phys. **135**, 154101 (2011).
[44]V. Lacivita, M. Rerat, R. Orlando, M. Ferrero, and R. Dovesi, J. Chem. Phys. **136**, 114101 (2012).
[45]R. Dovesi, V. R. Saunders, C. Roetti, R. Orlando, C. M. Zicovich-Wilson, F. Pascale, B. Civalleri, K. Doll, N. M. Harrison, I. J. Bush *et al.*, CRYSTAL 2009 User's Manual (2009), see http://www.crystal.unito.it.
[46]S. Boys and F. Bernardi, Mol. Phys. **19**, 553 (1970).
[47]E. Davidson and D. Feller, Chem. Rev. **86**, 681 (1986).
[48]C. Adamo and V. Barone, J. Phys. Chem. B **110**, 6158 (1999).
[49]T. Shigenari and K. Abe, J Chem. Phys. **136**, 174504 (2012).
[50]S. Gough, Can. J. Chem. **50**, 3046 (1972).
[51]S. Casassa and C. Pisani, J. Chem. Phys. **116**, 9856 (2002).
[52]S. Casassa, P. Ugliengo, and C. Pisani, J. Chem. Phys. **106**, 8030 (1997).
[53]N. Materer, U. Starke, A. Barbieri, M. V. Hove, G. Somorjai, G. Kroes, and C. Minot, J. Phys. Chem. **99**, 6267 (1995).